Supplementary Material

Nucleobase carbonyl groups are poor Mg^{2+} inner-sphere binders but excellent monovalent ion binders—a critical PDB survey

Filip Leonarski[1,2], Luigi D'Ascenzo[2,3], and Pascal Auffinger[2,*]

[1] Swiss Light Source, Paul Scherrer Institut, Villigen PSI, 5232, Switzerland

[2] Architecture et Réactivité de l'ARN, Université de Strasbourg, Institut de Biologie Moléculaire et Cellulaire du CNRS, Strasbourg, 67084, France

[3] Department of Integrative Structural and Computational Biology, The Scripps Research Institute, La Jolla, CA 92037, USA

* To whom correspondence should be addressed. Tel: +33 388 41 70 49; Fax: +33 388 60 22 18; Email: p.auffinger@ibmc-cnrs.unistra.fr

Table of content:

About ribosomal PDB structures (resolutions ≤ 2.9 Å) and biological assembly choice:

The February 2017 PDB release contains 93 X-ray structures of ribosomes with resolutions ≤ 2.9 Å (**Table S1**) that comprise: *(i)* 7 *Thermus thermophilus* small subunits (30S), *(ii)* 1 *Deinococcus radiodurans* large subunit (50S), *(iii)* 44 *Haloarcula marismortui* large subunits (50S), *(iv)* 30 *Thermus thermophilus* 70S ribosomes, *(v)* 9 *Escherichia coli* 70S ribosomes and *(vi)* 2 *Saccharomyces cerevisiae* 80S ribosomes.

For the 41 ribosomal structures (70S and 80S) that are only available as mmCIF files, the biological assembly with the lowest average *B*-factor was retained for analysis (see **Table S1**). For the *T. thermophilus* 70S structures, numbering inconsistencies between the two or four assemblies resulting from in-house PDB annotations were found. When such discrepancies were noted, we chose to use the structure that has a numbering consistent with the 2D structures found at http://apollo.chemistry.gatech.edu/RibosomeGallery (Petrov et al. 2013) as noted in **Table S1**.

Thermus thermophilus (30S)

In this ensemble of seven structures, **2VQE** has the best resolution (2.5 Å; **Table S1**). All structures contain Zn^{2+}/Mg^{2+} and K^{+} has been assigned in six of them. For some of these structures, Ca^{2+}, Na^{+}, NH_4^{+}, Cl^{-} and acetate ions may also be present according to the crystallization conditions provided by the PDB. Both r-proteins S4 and S14 contain a zinc-finger domain (Wimberly et al. 2000).

Deinococcus radiodurans (50S)

5DM6 is given with a 2.9 Å resolution. Mg^{2+} is the only assigned ion. Zn^{2+} is not present since the zinc finger cysteine residues form disulfide bridges. Na^{+}, NH_4^{+}, spermidine and Cl^{-} may also be present according to the crystallization conditions noted in the PDB. But these ions were not assigned.

Haloarcula marismortui (50S)

In this ensemble of 44 structures, **1VQO** and **1VQ8** have the best resolutions (2.2 Å). Oddly, all these structures contain Cd^{2+} in replacement of Zn^{2+}. It was reported that the addition of 1 mM $CdCl_2$ was able to significantly improve the crystal growth of these 50S subunits (von Bohlen et al. 1991) —note that $CdCl_2$ has been used for crystallization of other ribosomal systems (Wimberly et al. 1999; Sigel et al. 2013). The four L24e, L37e, L37ae, and L44e r-proteins contain zing finger motifs. Four of these domains, where Cd^{2+} replaces Zn^{2+}, were identified (Klein et al. 2004). In all these r-proteins, Cd^{2+} is tetrahedrally bound to four cysteine sulfur atoms. An additional weak and suspicious Cd^{2+} binding site is also reported. For some of these structures, NH_4^{+} and acetate ions may be present according to the crystallization conditions noted in the PDB. The 1FFK (2.4 Å) crystallization conditions (Ban et al. 2000) indicate the use of following crystallization buffer: 1.2 M KCl, 0.5 M NH_4Cl, 100 mM KCH_3COO, 30 mM $MgCl_2$, 7% PEG 6000, 15 mM tris, 15 mM MES, and 1 mM $MgCl_2$ at pH 7.1. The crystals were then stabilized by transfer to a solution containing 12% PEG 6000, 22% ethylene glycol, 1.7 M NaCl, 0.5 M NH_4Cl, 100 mM KCH_3COO, 30 mM $MgCl_2$, and 1 mM $CdCl_2$ at pH 6.2.

This group of *H. marismortui* structures is very heterogeneous. In early structures, residue 1329:0 was wrongly assigned to an adenine as shown by $2F_o - F_c$ and $F_o - F_c$ maps (**Figure S12**). This error and other inaccuracies have been subsequently corrected in **4V9F** —a re-refinement of **1FFK** (Gabdulkhakov et al. 2013)— and in the structures marked as such in **Table S1**. The best

resolution structures with the corrected sequence are thus, **4V9F**, **1YHQ** and **3CC2** (2.4 Å). Modified nucleotides are assigned in **4V9F**. Other details regarding the modifications introduced into the *H. marismortui* refinement process can be found in (Klein et al. 2004).

Twenty-four of these ribosome structures contain Sr^{2+}. The use of $SrCl_2$ is related to the crystallization of antibiotic/ribosome complexes and was shown to improve crystal quality (Zhang and Ferre-D'Amare 2014). In one study, it is mentioned that crystals were soaked with antibiotic in a buffer containing: 1.7 M NaCl, 0.5 M NH_4Cl, 1 mM $CdCl_2$, 100 mM KCH_3COO, 6.5 mM CH_3COOH and with either 30 mM $MgCl_2$, or 21 mM $MgCl_2$ and 30 mM $SrCl_2$, or no $MgCl_2$ and 100 mM $SrCl_2$ (Blaha et al. 2008). These conditions suggest that these ribosomes crystals include very high NaCl and NH_4Cl concentrations. The best resolution structure with Sr^{2+} and the corrected sequence is **3CCM** (2.55 Å).

Note that *H. marismortui* structures contain single ribosomal RNA chains, which are labeled in some structures “chain 0” and “chain A” in others. Here, these chains were considered equivalent.

Thermus thermophilus (70S)

In this ensemble of 30 structures, **4Y4O** has the best resolution (2.3 Å). Zn^{2+} is present in 29 structures.

Escherichia coli (70S)

In this ensemble of 9 structures, **4YBB** has the best resolution (2.1 Å as indicated in the PDB). It is also currently the best resolution of all ribosomal structures and contains a full array of modified nucleotides — note that the original publication mentions a 2.4 Å resolution (Noeske et al. 2015). For **4YBB**, a strong discrepancy between the *B*-factors of both assemblies present in the crystal unit must be noted (average *B*-factors around ≈67 and ≈123 $Å^2$ for assembly 1 and 2, respectively). As such, we limited our analysis to the first biological assembly. Besides 463 Mg^{2+} and 3 Zn^{2+} for the two assemblies, **4YBB** contains also acetate, 1,2-ethanediol, di(hydroxyethyl)ether, putrescine, spermidine, MPD, TRIS, tetraethylene- and pentaethylene-glycol. On the average, for all other *E. coli* ribosomes in **Table S1**, one Zn^{2+} and 180 to 240 Mg^{2+} are present in each assembly.

Saccharomyces cerevisiae (80S)

The best resolution structure is **4U4R** (2.8 Å). The two structures of this ensemble comprise each eight Zn^{2+}, ≈700 Mg^{2+} and ≈500 osmium hexamine per biological assembly. Crystallization protocols are given in reference (Ben-Shem et al. 2011).

Crystallization buffers

To correctly analyze crystal structures, it is important to be informed about all the molecules present in purification and crystallization buffers. Some buffers frequently used for ribosome assembly and translation are polymix (Jelenc and Kurland 1979) and HiFi (Gromadski and Rodnina 2004).

- Polymix buffer: 5 mM $Mg(OAc)_2$ or 14 mM $Mg(OAc)_2$ and 95 mM KCl, 5 mM NH_4Cl, 8 mM putrescine,1 mM spermidine, 1 mM DTT (2,3-dihydroxy-1,4-dithiobutane or dithioerythritol), 5 mM K_2HPO_4, and 0.5 mM $CaCl_2$.
- HiFi buffer: 3.5 mM $MgCl_2$ or 14 mM $MgCl_2$ and 30 mM KCl, 70 mM NH_4Cl, 8 mM putrescine, 0.5 mM spermidine, 1 mM DTT, and 50 mM Tris–HCl, pH 7.5.

Occupancy issues

Oddly, some structures have included Mg^{2+} ions with occupancies above 1.0 or very low *B*-factors that might hint to the presence of K^{+}/Ca^{2+}/Sr^{2+} or transition metals and not to the presence of Mg^{2+}. See for example the Zn^{2+} ion suggested to be present in the RNA part of some ribosomes (Leonarski et al. 2017). Taking these ions into account would not be beneficial to our statistical analysis. Consequently, they were excluded from this survey. For instance, 1FJG and 1N32 display Mg^{2+} occupancies in the 0.22–1.47 range (Carter et al. 2000; Ogle et al. 2002) and 4V9D, 4V51, 4U26, 4U27, 4U1V, 4V9P and 4V9O display water and Mg^{2+} with *B*-factors ≤ 1.0 $Å^2$. In 4V9D, 262 out of 498 Mg^{2+} and 798 out ouf 802 waters have *B*-factors ≤ 1.0 $Å^2$.

Table S1: **List of PDB ribosomal structures with resolutions ⩽ 2.9 Å.** The best resolution structures in each category are highlighted in blue. In each category, structures are ordered according to PDB deposition date (first criterion), best resolution (second criterion) and best *R-free* (third criterion). The 5J5B and 5J7L structures were excluded given specific difficulties related to the authors very peculiar encoding of the associated mmCIF files. This table is an updated version of **Table S1** in reference (Leonarski et al. 2017) and comprises all structures with resolutions ≤ 2.9 Å instead of ≤ 3.0 Å.

PDB code	Deposited	Res. (*R*-Free)	Residue count	Ions	Reference
T. Thermophilus (30S) *— 7 structures*					
2UUB	03/2007	2.80 (0.24)	4086	Zn^{2+}, Mg^{2+}, K^{+}	(Weixlbaumer et al. 2007)
2UUA	03/2007	2.90 (0.25)	4086	Zn^{2+}, Mg^{2+}, K^{+}	(Weixlbaumer et al. 2007)
2UXC	03/2007	2.90 (0.26)	4086	Zn^{2+}, Mg^{2+}, K^{+}	(Dunham et al. 2007)
2VQE	03/2008	2.50 (0.28)	4086	Zn^{2+}, Mg^{2+}, K^{+}	(Kurata et al. 2008)
2VQF	03/2008	2.90 (0.26)	4086	Zn^{2+}, Mg^{2+}, K^{+}	(Kurata et al. 2008)
3T1Y	07/2011	2.80 (0.27)	4065	Zn^{2+}, Mg^{2+}	(Vendeix et al. 2012)
4B3M	07/2012	2.90 (0.25)	4072	Zn^{2+}, Mg^{2+}, K^{+}	(Perez-Fernandez et al. 2014)
D. radiodurans (50S) *— 1 structure*					
5DM6	09/2015	2.90 (0.27)	6490	Mg^{2+}	(Kaminishi et al. 2015)
H. marismortui (50S) *— with wrong adenine at position 1329 (see **Figure S1**) — 22 structures*					
1FFK	07/2000	2.40 (0.26)	6825	Cd^{2+}, Mg^{2+}, K^{+}	(Ban et al. 2000)
1JJ2	07/2001	2.40 (0.22)	7279	Cd^{2+}, Mg^{2+}, K^{+}, Na^{+}, Cl^{-}	(Klein et al. 2001)
1M90	07/2002	2.80 (0.22)	7282	Cd^{2+}, Mg^{2+}, K^{+}, Na^{+}, Cl^{-}	(Hansen et al. 2002)
1QVG	08/2003	2.90 (0.26)	7288	Cd^{2+}, Mg^{2+}, K^{+}, Na^{+}, Cl^{-}	(Schmeing et al. 2003)
1S72	01/2004	2.40 (0.22)	7464	Cd^{2+}, Mg^{2+}, K^{+}, Na^{+}, Cl^{-}	(Klein et al. 2004)
1VQO[a]	12/2004	2.20 (0.25)	7478	Cd^{2+}, Sr^{2+}, Mg^{2+}, K^{+}, Na^{+}, Cl^{-}	(Schmeing et al. 2005a)
1VQ8[a]	12/2004	2.20 (0.25)	7479	Cd^{2+}, Sr^{2+}, Mg^{2+}, K^{+}, Na^{+}, Cl^{-}	(Schmeing et al. 2005a)
1VQP	12/2004	2.25 (0.25)	7483	Cd^{2+}, Sr^{2+}, Mg^{2+}, K^{+}, Na^{+}, Cl^{-}	(Schmeing et al. 2005a)
1VQK	12/2004	2.30 (0.25)	7480	Cd^{2+}, Sr^{2+}, Mg^{2+}, K^{+}, Na^{+}, Cl^{-}	(Schmeing et al. 2005a)
1VQL	12/2004	2.30 (0.25)	7482	Cd^{2+}, Sr^{2+}, Mg^{2+}, K^{+}, Na^{+}, Cl^{-}	(Schmeing et al. 2005a)
1VQM	12/2004	2.30 (0.25)	7482	Cd^{2+}, Sr^{2+}, Mg^{2+}, K^{+}, Na^{+}, Cl^{-}	(Schmeing et al. 2005a)
1VQN	12/2004	2.40 (0.25)	7484	Cd^{2+}, Sr^{2+}, Mg^{2+}, K^{+}, Na^{+}, Cl^{-}	(Schmeing et al. 2005b)
1VQ9	12/2004	2.40 (0.26)	7480	Cd^{2+}, Sr^{2+}, Mg^{2+}, K^{+}, Na^{+}, Cl^{-}	(Schmeing et al. 2005a)
1VQ7	12/2004	2.50 (0.24)	7482	Cd^{2+}, Mg^{2+}, K^{+}, Na^{+}, Cl^{-}	(Schmeing et al. 2005b)
1VQ5	12/2004	2.60 (0.24)	7482	Cd^{2+}, Mg^{2+}, K^{+}, Na^{+}, Cl^{-}	(Schmeing et al. 2005a)
1VQ4	12/2004	2.70 (0.23)	7482	Cd^{2+}, Mg^{2+}, K^{+}, Na^{+}, Cl^{-}	(Schmeing et al. 2005a)
1VQ6	12/2004	2.70 (0.23)	7483	Cd^{2+}, Mg^{2+}, K^{+}, Na^{+}, Cl^{-}	(Schmeing et al. 2005b)
2OTL	02/2007	2.70 (0.25)	7462	Cd^{2+}, Mg^{2+}, K^{+}, Na^{+}, Cl^{-}	(Schroeder et al. 2007b)
2OTJ	02/2007	2.90 (0.24)	7463	Cd^{2+}, Mg^{2+}, K^{+}, Na^{+}, Cl^{-}	(Schroeder et al. 2007b)
2QEX	06/2007	2.90 (0.24)	7320	Cd^{2+}, Mg^{2+}, K^{+}, Na^{+}, Cl^{-}	(Schroeder et al. 2007a)
3CPW	04/2008	2.70 (0.23)	7334	Cd^{2+}, Sr^{2+}, Mg^{2+}, K^{+}, Na^{+}, Cl^{-}	(Ippolito et al. 2008)
3OW2	09/2010	2.70 (0.25)	6801	Cd^{2+}, Sr^{2+}, Mg^{2+}, K^{+}, Na^{+}, Cl^{-}	—
H. marismortui (50S) *— with correct guanine at position 1329 (see (Leonarski et al. 2017)) — 22 structures*					
1YHQ	01/2005	2.40 (0.23)	7480	Cd^{2+}, Sr^{2+}, Mg^{2+}, K^{+}, Na^{+}, Cl^{-}	(Tu et al. 2005)
1YIJ	01/2005	2.60 (0.22)	7481	Cd^{2+}, Mg^{2+}, K^{+}, Na^{+}, Cl^{-}	(Tu et al. 2005)
1YI2	01/2005	2.65 (0.21)	7481	Cd^{2+}, Mg^{2+}, K^{+}, Na^{+}, Cl^{-}	(Tu et al. 2005)
1YIT	01/2005	2.80 (0.22)	7478	Cd^{2+}, Mg^{2+}, K^{+}, Na^{+}, Cl^{-}	(Tu et al. 2005)
1YJ9	01/2005	2.80 (0.24)	7478	Cd^{2+}, Mg^{2+}, K^{+}, Na^{+}, Cl^{-}	(Tu et al. 2005)
1YJW	01/2005	2.90 (0.22)	7481	Cd^{2+}, Mg^{2+}, K^{+}, Na^{+}, Cl^{-}	(Tu et al. 2005)
3CC2	02/2008	2.40 (0.23)	7517	Cd^{2+}, Mg^{2+}, K^{+}, Na^{+}, Cl^{-}	(Blaha et al. 2008)
3CCM	02/2008	2.55 (0.24)	7517	Cd^{2+}, Sr^{2+}, Mg^{2+}, K^{+}, Na^{+}, Cl^{-}	(Blaha et al. 2008)
3CC7	02/2008	2.70 (0.23)	7517	Cd^{2+}, Sr^{2+}, Mg^{2+}, K^{+}, Na^{+}, Cl^{-}	(Blaha et al. 2008)
3CCJ	02/2008	2.70 (0.23)	7517	Cd^{2+}, Sr^{2+}, Mg^{2+}, K^{+}, Na^{+}, Cl^{-}	(Blaha et al. 2008)
3CC4	02/2008	2.70 (0.24)	7517	Cd^{2+}, Sr^{2+}, Mg^{2+}, K^{+}, Na^{+}, Cl^{-}	(Blaha et al. 2008)
3CCE	02/2008	2.75 (0.23)	7517	Cd^{2+}, Sr^{2+}, Mg^{2+}, K^{+}, Na^{+}, Cl^{-}	(Blaha et al. 2008)
3CD6	02/2008	2.75 (0.24)	7520	Cd^{2+}, Sr^{2+}, Mg^{2+}, K^{+}, Na^{+}, Cl^{-}	(Blaha et al. 2008)
3CCU	02/2008	2.80 (0.22)	7517	Cd^{2+}, Sr^{2+}, Mg^{2+}, K^{+}, Na^{+}, Cl^{-}	(Blaha et al. 2008)
3CCL	02/2008	2.90 (0.22)	7517	Cd^{2+}, Sr^{2+}, Mg^{2+}, K^{+}, Na^{+}, Cl^{-}	(Blaha et al. 2008)
3CCV	02/2008	2.90 (0.22)	7517	Cd^{2+}, Sr^{2+}, Mg^{2+}, K^{+}, Na^{+}, Cl^{-}	(Blaha et al. 2008)
3CCQ	02/2008	2.90 (0.23)	7517	Cd^{2+}, Sr^{2+}, Mg^{2+}, K^{+}, Na^{+}, Cl^{-}	(Blaha et al. 2008)
3CMA	03/2008	2.80 (0.24)	7522	Cd^{2+}, Sr^{2+}, Mg^{2+}, K^{+}, Na^{+}, Cl^{-}	(Simonovic and Steitz 2008)
3G6E	02/2009	2.70 (0.23)	7217	Cd^{2+}, Sr^{2+}, Mg^{2+}, K^{+}, Na^{+}, Cl^{-}	(Gurel et al. 2009)
3G71	02/2009	2.85 (0.23)	7217	Cd^{2+}, Sr^{2+}, Mg^{2+}, K^{+}, Na^{+}, Cl^{-}	(Gurel et al. 2009)
3I56	07/2009	2.90 (0.24)	7217	Cd^{2+}, Sr^{2+}, Mg^{2+}, K^{+}, Na^{+}, Cl^{-}	(Gurel et al. 2009)
4V9F[b]	02/2012	2.40 (0.21)	7583[c,d]	Cd^{2+}, Mg^{2+}, K^{+}, Na^{+}, Cl^{-}	(Gabdulkhakov et al. 2013)
T. thermophilus (70S) *— 30 structures*					

4V51	07/2006	2.80 (0.31)	21886[c,e]	Zn^{2+}, Mg^{2+}	(Selmer et al. 2006)
4V8I	12/2011	2.70 (0.25)	21484[c,e]	Zn^{2+}, Mg^{2+}	(Polikanov et al. 2012)
4V9H	03/2013	2.86 (0.25)	11728[c,d]	Mg^{2+}	(Tourigny et al. 2013)
1VY5	05/2014	2.55 (0.28)	21748[c,e]	Zn^{2+}, Mg^{2+}, K^{+}	(Polikanov et al. 2014b)
1VY4	05/2014	2.60 (0.26)	21748[c,e]	Zn^{2+}, Mg^{2+}, K^{+}	(Polikanov et al. 2014b)
1VY7	05/2014	2.80 (0.28)	21602[c,e]	Zn^{2+}, Mg^{2+}, K^{+}	(Polikanov et al. 2014b)
1VY6	05/2014	2.90 (0.29)	21448[c,e]	Zn^{2+}, Mg^{2+}, K^{+}	(Polikanov et al. 2014b)
4W2E	06/2014	2.90 (0.30)	11638[c,d]	Zn^{2+}, Mg^{2+}	(Gagnon et al. 2014)
4W2G	09/2014	2.55 (0.27)	21748[c,e]	Zn^{2+}, Mg^{2+}, K^{+}	(Polikanov et al. 2014a)
4W2H	09/2014	2.70 (0.26)	21596[c,e]	Zn^{2+}, Mg^{2+}, K^{+}	(Polikanov et al. 2014a)
4W2I	09/2014	2.70 (0.26)	21748[c,e]	Zn^{2+}, Mg^{2+}, K^{+}	(Polikanov et al. 2014c)
4W2F	10/2014	2.40 (0.28)	21748[c,e]	Zn^{2+}, Mg^{2+}, K^{+}	(Polikanov et al. 2014a)
4WPO	10/2014	2.80 (0.25)	24064[c,e]	Zn^{2+}, Mg^{2+}, K^{+}	(Lin et al. 2015)
4WQF	10/2014	2.80 (0.26)	23898[c,e]	Zn^{2+}, Mg^{2+}	(Lin et al. 2015)
4WQU	10/2014	2.80 (0.26)	23918[c,e]	Zn^{2+}, Mg^{2+}	(Lin et al. 2015)
4WQY	10/2014	2.80 (0.27)	23760[c,e]	Zn^{2+}, Mg^{2+}, K^{+}	(Lin et al. 2015)
4Y4O[b]	02/2015	2.30 (0.25)	21468[c,e]	Zn^{2+}, Mg^{2+}	(Polikanov et al. 2015a)
4Y4P	02/2015	2.50 (0.28)	21748[c,e]	Zn^{2+}, Mg^{2+}, K^{+}	(Seefeldt et al. 2016)
4Z3S	03/2015	2.65 (0.27)	21748[c,e]	Zn^{2+}, Mg^{2+}, K^{+}	(Polikanov et al. 2015b)
4Z8C[j]	04/2015	2.90 (0.25)	21482[c,e]	Zn^{2+}, Mg^{2+}	(Roy et al. 2015)
5DOY	09/2015	2.60 (0.28)	21754[c,e]	Zn^{2+}, Mg^{2+}, K^{+}	(Polikanov et al. 2015b)
5FDV	12/2015	2.80 (0.24)	20986[c,e]	Zn^{2+}, Mg^{2+}	(Seefeldt et al. 2016)
5F8K	12/2015	2.80 (0.29)	20948[c,e]	Zn^{2+}, Mg^{2+}, K^{+}	(Seefeldt et al. 2016)
5FDU	12/2015	2.90 (0.23)	20974[c,e]	Zn^{2+}, Mg^{2+}	(Seefeldt et al. 2016)
5HD1[j]	01/2016	2.70 (0.27)	21484[c,e]	Zn^{2+}, Mg^{2+}	(Gagnon et al. 2016b)
5HCQ[j]	01/2016	2.80 (0.25)	21472[c,e]	Zn^{2+}, Mg^{2+}	(Gagnon et al. 2016b)
5HCR[j]	01/2016	2.80 (0.27)	21482[c,e]	Zn^{2+}, Mg^{2+}	(Gagnon et al. 2016b)
5HCP[j]	01/2016	2.89 (0.27)	21474[c,e]	Zn^{2+}, Mg^{2+}	(Gagnon et al. 2016b)
5J4B	03/2016	2.60 (0.26)	21748	Zn^{2+}, Mg^{2+}, K^{+}	(Melnikov et al. 2016)
5J4C	03/2016	2.80 (0.27)	21748	Zn^{2+}, Mg^{2+}, K^{+}	(Melnikov et al. 2016)
5J8B	04/2016	2.60 (0.26)	11953	Zn^{2+}, Mg^{2+}	(Gagnon et al. 2016a)
E. coli (70S) *— 9 structures*					
4V9O	05/2013	2.90 (0.27)	45264[c,f]	Zn^{2+}, Mg^{2+}	(Pulk and Cate 2013)
4V9P	05/2013	2.90 (0.27)	44972[c,f]	Zn^{2+}, Mg^{2+}	(Pulk and Cate 2013)
4U27	06/2014	2.80 (0.26)	20808[c,e]	Zn^{2+}, Mg^{2+}	(Noeske et al. 2014)
4U26	06/2014	2.80 (0.27)	20810[c,e]	Zn^{2+}, Mg^{2+}	(Noeske et al. 2014)
4U20	06/2014	2.90 (0.28)	20794[c,e]	Zn^{2+}, Mg^{2+}	(Noeske et al. 2014)
4U24	06/2014	2.90 (0.26)	20794[c,e]	Zn^{2+}, Mg^{2+}	(Noeske et al. 2014)
4U25	06/2014	2.90 (0.26)	20794[c,e]	Zn^{2+}, Mg^{2+}	(Noeske et al. 2014)
4YBB[b]	02/2015	2.10 (0.23)	20744[c,e,h]	Zn^{2+}, Mg^{2+}	(Noeske et al. 2015)
5J5B[b]	04/2016	2.80 (0.20)	20745[c,e,h]	Zn^{2+}, Mg^{2+}	(Cocozaki et al. 2016)
S. cerevisiae (80S) *— 2 structures* [i]					
4U4R	07/2014	2.80 (0.25)	35344[c,g]	Zn^{2+}, Mg^{2+}	(Garreau de Loubresse et al. 2014)
4U3U	07/2014	2.90 (0.24)	35344[c,g]	Zn^{2+}, Mg^{2+}	(Garreau de Loubresse et al. 2014)

[a] Although these ribosomes have the best 2.2 Å resolution for *H. marismortui*, they embed assignment errors as shown in **Figure S1** and should be considered with caution.
[b] These structures include ribosomal modifications.
[c] These very large ribosomal structures are only available in mmCIF format in the PDB.
[d] These large structures contain one biological assembly (space group: P1211).
[e] These large structures contain two biological assemblies (space group: P212121).
[f] These large structures contain four biological assemblies (space group: P1211).
[g] These large structures contain two biological assemblies (space group: P1211).
[h] The *B*-factors of the first assembly are significantly higher than those of the second assembly that should consequently not be considered for further structural analysis.
[i] The numbering of these files are consistent with the 2D structures available at http://apollo.chemistry.gatech.edu/RibosomeGallery (Petrov et al. 2013).
[j] The numbering of these files follows sequence and is not aligned towards *E. coli* ribosome.
[k] Structure factors not available.

Table S2: **Extract of the "ener_lib.cif" file (dated 04-04-1995/31-05-2000) showing coordination distance restraint values associated with Mg^{2+}.** It is advised to always check this and similar libraries before starting a structure refinement. Such files and their documented use should be included in the deposited PDB data. Note also the too long Mg^{2+} to oxygen coordination distance restraint values highlighted in yellow (Leonarski et al. 2017).

```
# ------------------------------------------------------------------
#          ener_lib.cif          4-APR-95/31-MAY-00
# ------------------------------------------------------------------
#
data_energy
#
# ------------------------------------------------------------------
#     _dictionary_name        ciflibdic
#     _dictionary_version     2.0
# ------------------------------------------------------------------
…

# ---  BONDS ---
#
loop_
_lib_bond.atom_type_1
_lib_bond.atom_type_2
_lib_bond.type
_lib_bond.const
_lib_bond.length
_lib_bond.value_esd
#
#          _atom_type          atomic chemical type
#          _const              constant KBOND
#          _value              equilibrium length of this bond BOND0
#                              BOND - actual bond length
#
#                              ENERGY = KBOND * ( BOND - BOND0 )**2
#
#          Values for bond distances and sigmas are from (where it is possible):
#          International tables for crystallography
#          Volume C, 1992,
#          Edited by AJC Wilson
#          Published for IUCr by Kluwer Academic Publishers, Dordrecht/Boston/London
#          For carbon-carbon etc
#          Section: Typical Interatomic distances: Organic compounds
#          Authors: FH Allen, O. Kennard, DG Watson, L Brammer, AG Orpen and R Taylor
#          pages:   685-706
#
#          For metal radii and distances.
#          Section: Typical interatomic distances: Organometallic Compounds and
#          Coordination complexes of the d- and f-block metals
#          Authors: AG Orpen, L. Brammer, FH Allen, O Kennard, DG Watson and R Taylor
#          pages:   707-791
#
…
MG      .       metal           .       2.670   0.040
MG      NPA     metal   500.000 2.090   .
MG      NPB     metal   500.000 2.090   .
MG      OHA     metal   500.000 2.150   .       # ?
MG      OHB     metal   500.000 2.150   .       # ?
MG      OHC     metal   500.000 2.150   .       # ?
MG      O       metal   500.000 2.180   .       # ?
…
```

Table S3. **MgRNA database Mg^{2+} binding sites involving O_r atoms and correspondence with present study**. No "*prior-knowledge*" binding sites could be identified for these atoms suggesting that O_r atoms do generally not participate in Mg^{2+} binding sites. See also **Tables 2/S4** for Mg^{2+} binding sites centered on O_b and N_b atoms, respectively. With present state of structural knowledge, Mg^{2+} binding to O_r atoms seems only to occur with terminal nucleotides (see text and **Fig. S6**).

Order number	Potential binding sites[a]	MgRNA occurrence	Prior-knowledge (this study)
1.	O_r	22	*Poor stereochemistry*
2.	$2O_r$	6	*Poor occurrence and stereochemistry*
3.	$O_r.O_b$	1	*Poor occurrence and stereochemistry*
4.	$2O_r.N_b$	1	*Poor occurrence and stereochemistry*
5.	$2O_r.2O_b$	1	*Poor occurrence and stereochemistry*
6.	$O_{ph}.O_r$	49	*Poor stereochemistry*
7.	$O_{ph}.2O_r$	8	*Poor occurrence and stereochemistry*
8.	$O_{ph}.O_r.2O_b$	1	*Poor occurrence and stereochemistry*
9.	*cis*-$2O_{ph}.O_r$	36	*Poor stereochemistry*
10.	*cis*-$2O_{ph}.2O_r$	2	*Poor occurrence and stereochemistry*
11.	*cis*-$2O_{ph}.O_r.O_b$	2	*Poor occurrence and stereochemistry*
12.	*fac*-$3O_{ph}.O_r$	3	*Poor occurrence and stereochemistry*
13.	*mer*-$3O_{ph}.O_r$	19	*Poor stereochemistry*

[a] The O_{ph} (OP1/2: anionic phosphate oxygen atoms), O_r (O2', O4': ribose oxygen atoms; O3', O5': phosphodiester oxygen atoms), Ob (O2, O4, O6: nucleobase carbonyl oxygen atoms) and N_b (essentially N7 purine nitrogen atoms) are derived from the MgRNA nomenclature (Zheng et al. 2015).

Table S4. **MgRNA database Mg^{2+} binding sites involving N_b atoms and correspondence with data from a preceding study** (Leonarski et al. 2017). Examples of potential "*prior-knowledge*" binding sites are highlighted in grey and reference to figures are given. See also **Table 2/S3** for Mg^{2+} binding sites centered on O_b and O_r atoms, respectively.

Order number	Potential binding sites[a]	MgRNA occurrence	Prior-knowledge from (Leonarski et al. 2017)	
1.	N_b	284	**Figs 4A/4B**	
2.	$O_r.O_b$	1	*Poor occurrence and stereochemistry*	—
3.	$2N_b$	158	*Monovalent ion or transition metal binding site*	—
4.	$2O_b.N_b$	1	*Poor occurrence and stereochemistry*	—
5.	$O_b.2N_b$	3	*Poor occurrence and stereochemistry*	—
6.	$2O_r.N_b$	1	*Poor occurrence and stereochemistry*	—
7.	$O_{ph}.N_b$	134	**Fig. S8A** (*cis*-) **Fig. S8B** (*trans*-)	
7.[b]	$O_{coo}.N_b$	—	Not present in MgRNA **Fig. 7B** (*trans*-)	
8.	*cis*-$2O_{ph}.N_b$	118	**Fig. 7A/S7**	

[a] The O_{ph} (OP1/2: anionic phosphate oxygen atoms), O_r (O2', O4': ribose oxygen atoms; O3', O5': phosphodiester oxygen atoms), Ob (O2, O4, O6: nucleobase carbonyl oxygen atoms) and N_b (essentially N7 purine nitrogen atoms) are derived from the MgRNA nomenclature (Zheng et al. 2015).
[b] O_{coo} corresponds to the anionic oxygen atom of an Asp/Glu carboxyl/ate group and is not referenced by MgRNA.

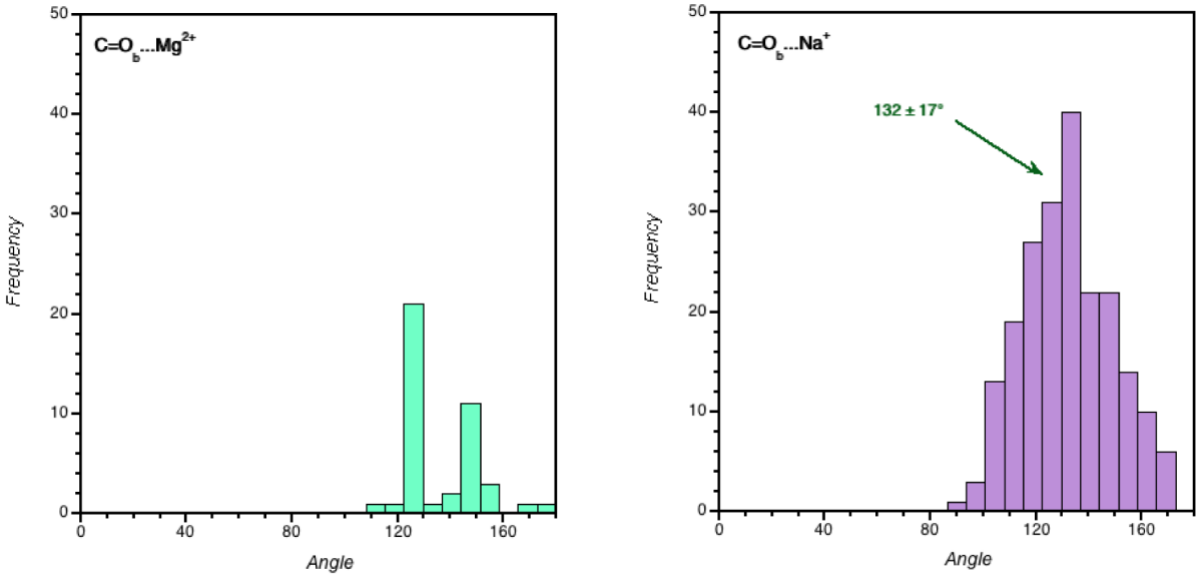

Figure S1. C=O$_b$…Mg^{2+}/Na$^+$ angle histograms derived from the CSD. (Left) C=O$_b$…Mg^{2+} and (Right) C=O$_b$…Na$^+$ histograms. The average C=O$_b$…Na$^+$ angle is 132 ± 17°. These histograms support the presence of the exclusion cone sketched **Fig. 2**. Note that in the CSD, the structural environments are highly heterogeneous and the number of O$_b$-to-Mg^{2+} contacts is ¼ that of O$_b$-to-Na$^+$ contacts.

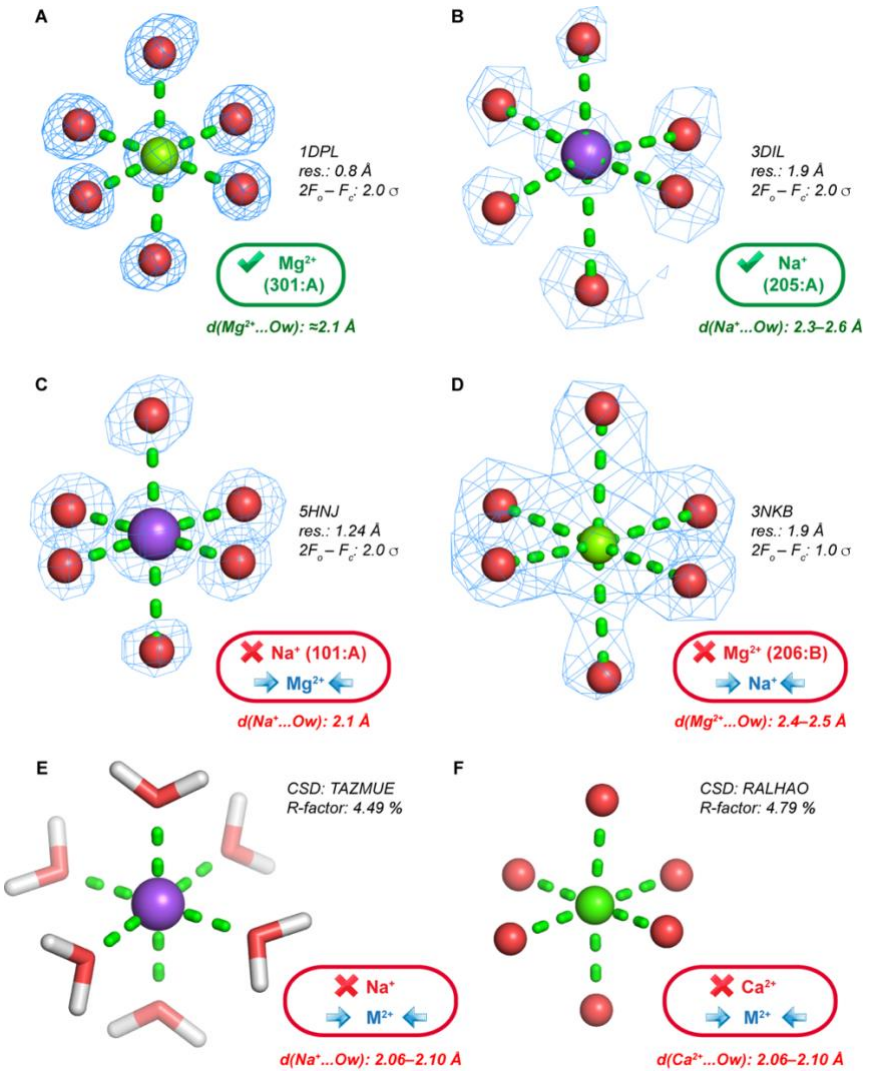

Figure S2. Stereochemically correct and unconvincing hexahydrated Mg^{2+}/Na^{+}/Ca^{2+} derived from PDB and CSD X-ray structures. (**A**) *d*(Mg^{2+}…Ow) ≈2.1 Å are compatible with Mg^{2+}. (**B**) *d*(Na^{+}…Ow) ≈2.4 Å are compatible with Na^{+}. (**C**) *d*(Na^{+}…Ow) ≈2.1 Å hint to Mg^{2+}. (**D**) *d*(Mg^{2+}…Ow) ≈2.4 Å hint to Na^{+}. (**E**) With respect to its ≈2.1 Å coordination distance d, this ion from the CSD should not be assigned to Na^{+}. (**F**) Similarly, with respect to a ≈2.1 Å coordination distance characteristic of Mg^{2+}, this ion should not be assigned to Ca^{2+}.

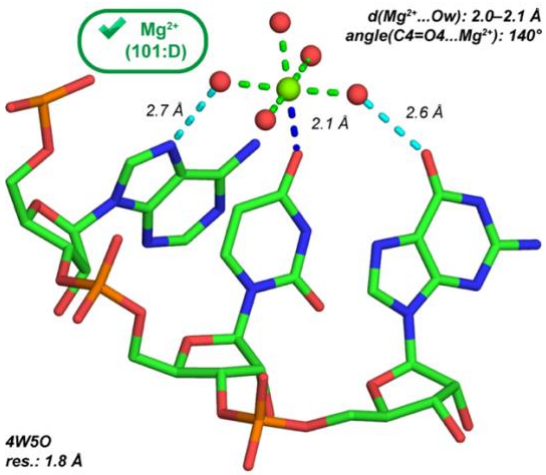

Figure S3. $Mg(H_2O)_5^{2+}$ bound to the (U)O4 atom of a ApUpG sequence involves water mediated contacts. This coordination pattern, also observed in two other structures (PDBid: 4Z4D/E) is similar to that shown in **Fig. 3E** where the binding sequence is GpGpG.

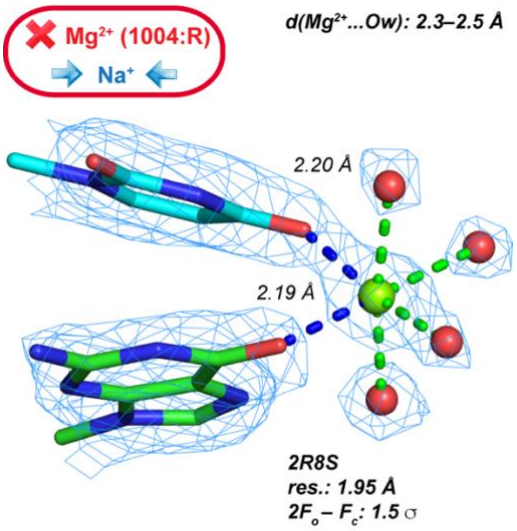

Figure S4. Unconvincing *cis*-2O$_b$ Mg^{2+} binding site. Coordination distances to water hint to Na^+. The ≈2.18 Å distances to the two O_b atoms point to the use of distance restraints — see **Fig. 6C** in (Leonarski et al. 2017) as well as **Table S2**.

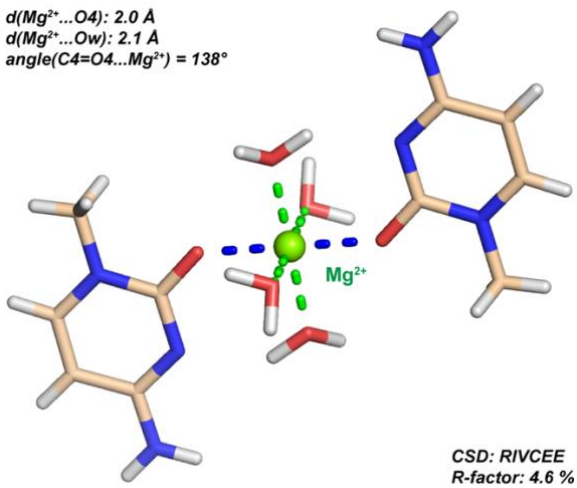

Figure S5. High-resolution CSD structure showing a *trans*-2O$_b$ Mg^{2+} binding motif (Gong et al. 2013); see also (Marino et al. 2016). This motif is rare and has not been observed, with appropriate stereochemistry, in PDB structures. Note that the CSD crystallisation conditions usually largely difer from those used in biomolecular systems.

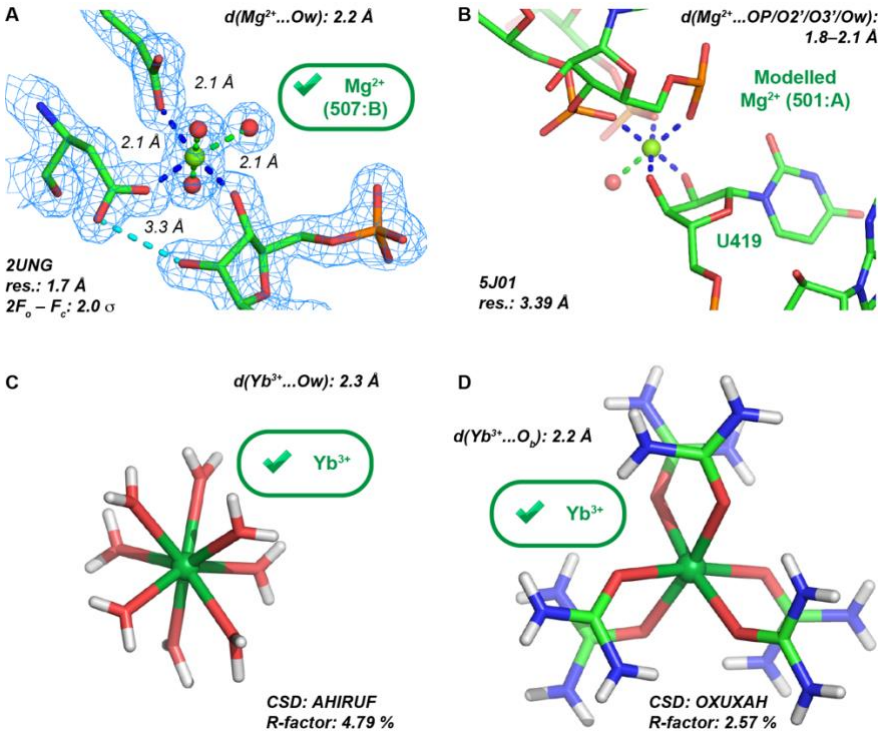

Figure S6. Mg^{2+} rarely binds to O2'/O3' hydroxyl groups; Yb^{3+} is rarely hexacoordinated. (**A**) From this unfrequent arrangement ($2O_{coo}.O_r$), it is suggested that the O3' atom coordinated to Mg^{2+} is deprotonated and may carry a negative charge (Gan et al. 2008). (**B**) A Mg^{2+} binding to the O2'/O3' atoms of a terminal residue ($3O_{ph}.2O_r$) modeled based on anomalous diffraction data of a group II intron Yb^{3+} derivative structure (Costa et al. 2016). (**C**) A Yb^{3+} with eight 1st shell water molecules commonly observed in the CSD (Thuery 2009). (**D**) A rare Yb^{3+} with six 1st shell oxygen atoms extracted from a CSD structure (Lundberg et al. 2010).

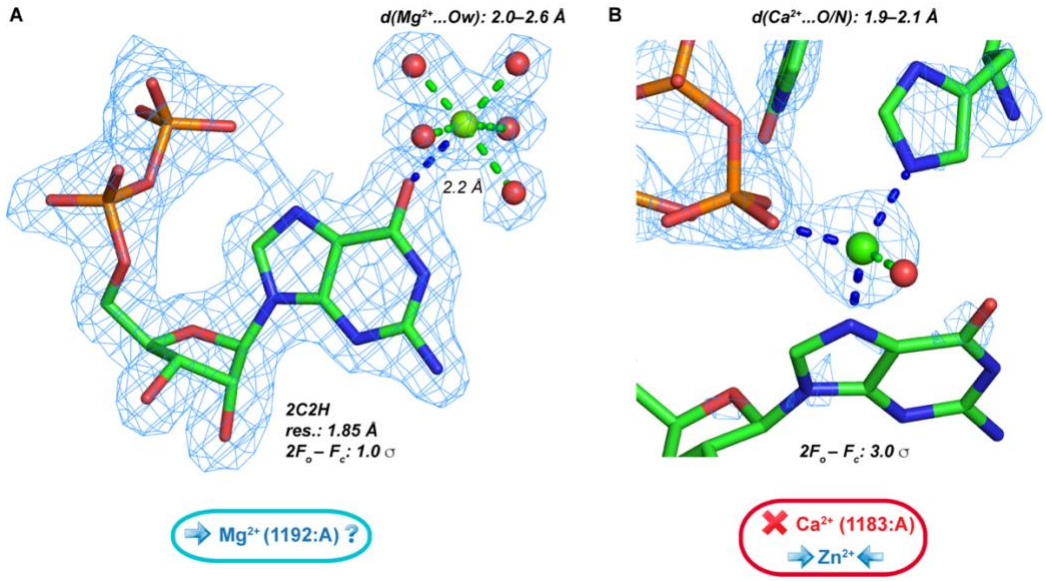

Figure S7. Unconvincing Mg^{2+} binding to a GDP containing DNA structure. (**A**) This Mg^{2+} binding to an O_b atom is unique among all PDB structures of nucleobase containing metabolites with resolution ≤ 2.9 Å. (**B**) In the same structure, 12 tetrahedral coordinated Ca^{2+} were assigned. This ion is more likely Zn^{2+} since Ca^{2+} has in all instances a coordination number ≥ 6.

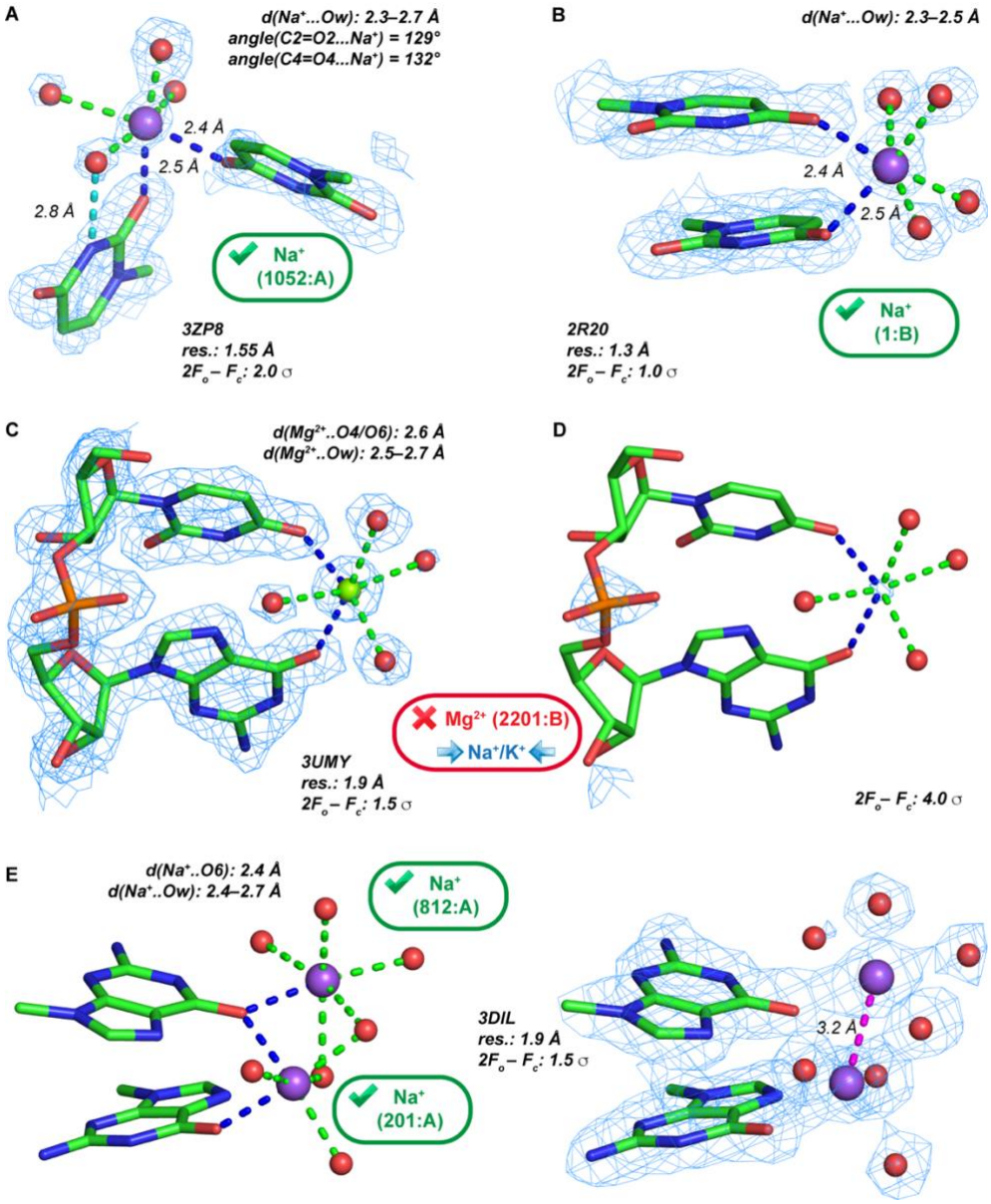

Figure S8. Na^+ binding sites and a dimetallic Na^+ cluster in PDB structures with resolution < 2.0 Å. (**A**) A *cis*-$2O_b$ Na^+ binding site ressembling the *cis*-$O_{ph}.O_b$ Mg^{2+} site shown **Fig. 4B**. (**B**) A frequent *cis*-$2O_b$ Na^+ site linking two consecutive uridines and ressembling the *cis*-$O_{ph}.O_b$ Mg^{2+} site shown in **Fig. S4**. (**C**) Improbable *cis*-$2O_b$ Mg^{2+} binding site with coordination distances hinting to Na^+ or K^+. (**D**) The same binding site with densities shown at a 4.0 sigma level. The octahedral coordination suggests the presence of Na^+ while both, the residual density at the 4.0 sigma level —ion not shown— and the longer coordination distances, suggests the presence of K^+. In this case, anomalous diffraction data would be required for unambiguous ion assignment; see (Olieric et al. 2016). (**E**) Two views of a dimetallic Na^+ cluster associated with a head-to-tail guanine arrangement similar to those described in (Leonarski et al. 2017).

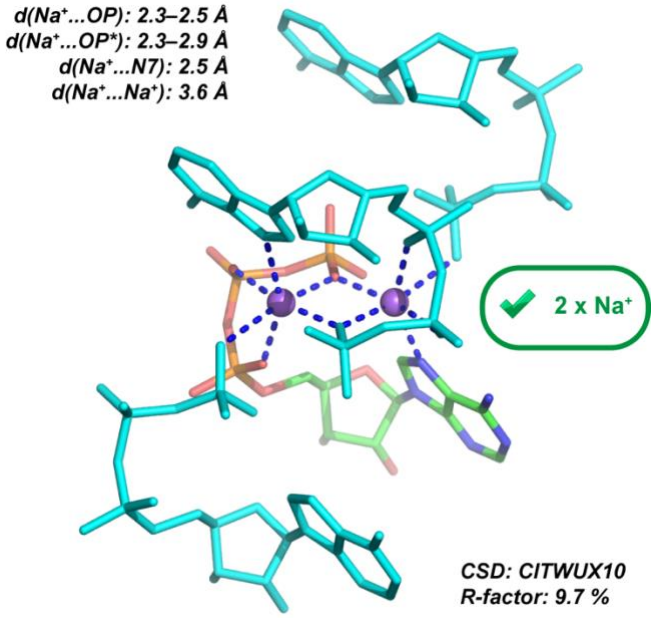

Figure S9. CSD structure of Na_2ATP with a dimetallic Na^+ cluster (Kennard et al. 1970; Sugawara et al. 1991)**.** Each hexacoordinated Na^+ is surrounded by five phosphate groups and one N7 atom. The ATP molecules in cyan are crystallographic symmetrics. OP* indicates coordination distances to a symmetric molecule.

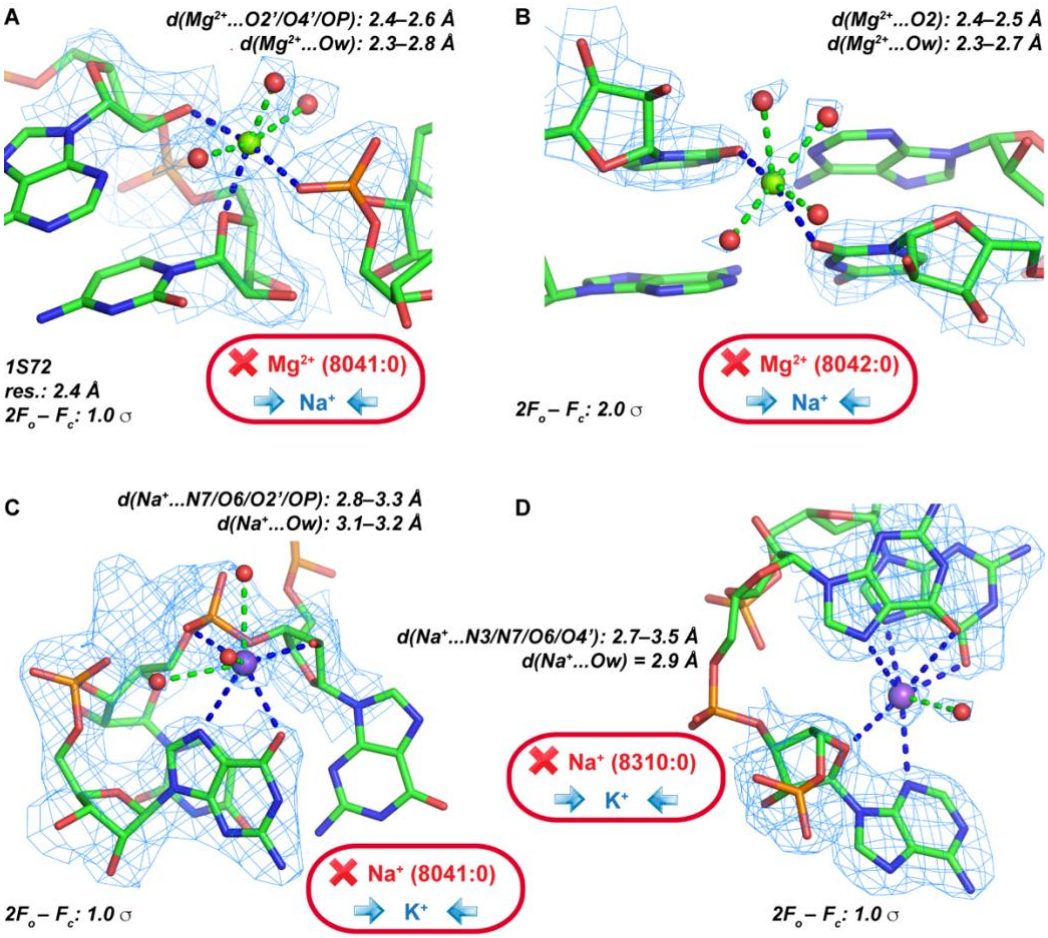

Figure S10. Unconvincing Mg^{2+} and Na^{+} binding sites derived from *H. marismortui* 50S structure. (**A**/**B**) Coordination distances exclude Mg^{2+} and suggest the presence of Na^{+} (**C**/**D**) Both, coordination distances and irregular coordination patterns exclude Mg^{2+} and point to the presence of K^{+}.

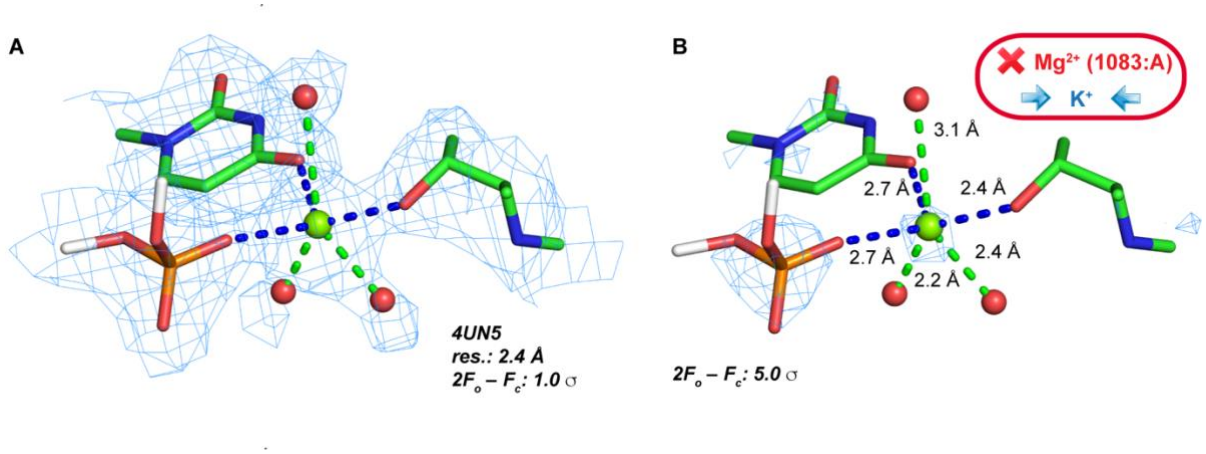

Figure S11. Unconvincing Mg^{2+} with a high sigma peak is probably K^+ (Anders et al. 2014)**.** (**A**) This hexacoordinated Mg^{2+} is bound to an OP, a (U)O4, a threonine hydroxyl group and three water molecules. Note that the two water molecules with short coordination distances are not placed at the center of the corresponding electron density patterns. (**B**) The Mg^{2+} density is still visible at 5.0 sigma. Therefore, this density pattern should rather be associated with K^+ as suggested in (Olieric et al. 2016).

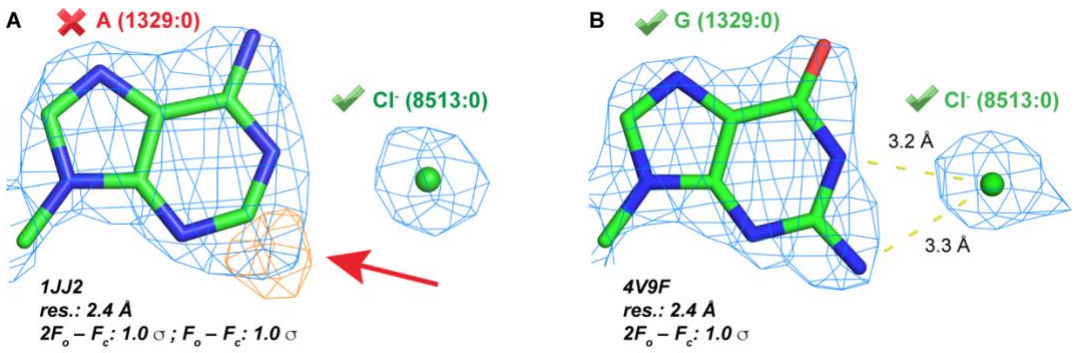

Figure S12. Nucleotide assignment error in early *H. marismortui* 50S structures. (**A**) Although a density for an amino N2 group is clearly visible in the $F_o - F_c$ map (red arrow), this nucleotide has been wrongly assigned to an adenine in 1FFK, 1JJ2 and related structures (**Table S1**) at odds with a Cl^- ion bound to its Watson-Crick edge (Auffinger et al. 2004; D'Ascenzo and Auffinger 2016). (**B**) This error has been corrected in 4V9F and related structures (**Table S1**).

Reference

Anders C, Niewoehner O, Duerst A, Jinek M. 2014. Structural basis of PAM-dependent target DNA recognition by the Cas9 endonuclease. *Nature* **513**: 569-573.

Auffinger P, Bielecki L, Westhof E. 2004. Anion binding to nucleic acids. *Structure* **12**: 379-388.

Ban N, Nissen P, Hansen J, Moore PB, Steitz TA. 2000. The complete atomic structure of the large ribosomal subunit at 2.4 Å resolution. *Science* **289**: 905-920.

Ben-Shem A, Garreau de Loubresse N, Melnikov S, Jenner L, Yusupova G, Yusupov M. 2011. The structure of the eukaryotic ribosome at 3.0 Å resolution. *Science* **334**: 1524-1529.

Blaha G, Gurel G, Schroeder SJ, Moore PB, Steitz TA. 2008. Mutations outside the anisomycin-binding site can make ribosomes drug-resistant. *J. Mol. Biol.* **379**: 505-519.

Carter AP, Clemons WM, Brodersen DE, Morgan-Warren RJ, Wimberly BT, Ramakrishnan V. 2000. Functional insights from the structure of the 30S ribosomal subunit and its interactions with antibiotics. *Nature* **407**: 340-348.

Cocozaki AI, Altman RB, Huang J, Buurman ET, Kazmirski SL, Doig P, Prince DB, Blanchard SC, Cate JH, Ferguson AD. 2016. Resistance mutations generate divergent antibiotic susceptibility profiles against translation inhibitors. *Proc. Natl. Acad. Sci. USA* **113**: 8188-8193.

Costa M, Walbott H, Monachello D, Westhof E, Michel F. 2016. Crystal structures of a group II intron lariat primed for reverse splicing. *Science* **354**.

D'Ascenzo L, Auffinger P. 2016. Anions in nucleic acid crystallography. *Methods Mol. Biol.* **1320**: 337-351.

Dunham CM, Selmer M, Phelps SS, Kelley AC, Suzuki T, Joseph S, Ramakrishnan V. 2007. Structures of tRNAs with an expanded anticodon loop in the decoding center of the 30S ribosomal subunit. *RNA* **13**: 817-823.

Gabdulkhakov A, Nikonov S, Garber M. 2013. Revisiting the *Haloarcula marismortui* 50S ribosomal subunit model. *Acta Cryst.* **D69**: 997-1004.

Gagnon MG, Lin J, Bulkley D, Steitz TA. 2014. Crystal structure of elongation factor 4 bound to a clockwise ratcheted ribosome. *Science* **345**: 684-687.

Gagnon MG, Lin J, Steitz TA. 2016a. Elongation factor 4 remodels the A-site tRNA on the ribosome. *Proc. Natl. Acad. Sci. USA* **113**: 4994-4999.

Gagnon MG, Roy RN, Lomakin IB, Florin T, Mankin AS, Steitz TA. 2016b. Structures of proline-rich peptides bound to the ribosome reveal a common mechanism of protein synthesis inhibition. *Nucleic Acids Res.* **44**: 2439-2450.

Gan J, Shaw G, Tropea JE, Waugh DS, Court DL, Ji X. 2008. A stepwise model for double-stranded RNA processing by ribonuclease III. *Mol. Microbiol.* **67**: 143-154.

Garreau de Loubresse N, Prokhorova I, Holtkamp W, Rodnina MV, Yusupova G, Yusupov M. 2014. Structural basis for the inhibition of the eukaryotic ribosome. *Nature* **513**: 517-522.

Gong Y, Hao Z, Li J, Wu T, Lin J. 2013. Mg(II)-induced second-harmonic generation based on bis-monodentate coordination mode of thiobarbiturate. *Dalton Trans.* **42**: 6489-6494.

Gromadski KB, Rodnina MV. 2004. Kinetic determinants of high-fidelity tRNA discrimination on the ribosome. *Mol. Cell* **13**: 191-200.

Gurel G, Blaha G, Moore PB, Steitz TA. 2009. U2504 determines the species specificity of the A-site cleft antibiotics: the structures of tiamulin, homoharringtonine, and bruceantin bound to the ribosome. *J. Mol. Biol.* **389**: 146-156.

Hansen JL, Schmeing TM, Moore PB, Steitz TA. 2002. Structural insights into peptide bond formation. *Proc. Natl. Acad. Sci. USA* **99**: 11670-11675.

Ippolito JA, Kanyo ZF, Wang D, Franceschi FJ, Moore PB, Steitz TA, Duffy EM. 2008. Crystal structure of the oxazolidinone antibiotic linezolid bound to the 50S ribosomal subunit. *J. Med. Chem.* **51**: 3353-3356.

Jelenc PC, Kurland CG. 1979. Nucleoside triphosphate regeneration decreases the frequency of translation errors. *Proc. Natl. Acad. Sci. USA* **76**: 3174-3178.

Kaminishi T, Schedlbauer A, Fabbretti A, Brandi L, Ochoa-Lizarralde B, He CG, Milon P, Connell SR, Gualerzi CO, Fucini P. 2015. Crystallographic characterization of the ribosomal binding site and molecular mechanism of action of Hygromycin A. *Nucleic Acids Res.* **43**: 10015-10025.

Kennard O, Isaacs NW, Coppola JC, Kirby AJ, Warren S, Motherwell WD, Watson DG, Wampler DL, Chenery DH, Larson AC et al. 1970. Three dimensional structure of adenosine triphosphate. *Nature* **225**: 333-336.

Klein DJ, Moore PB, Steitz TA. 2004. The roles of ribosomal proteins in the structure assembly, and evolution of the large ribosomal subunit. *J. Mol. Biol.* **340**: 141-177.

Klein DJ, Schmeing TM, Moore PB, Steitz TA. 2001. The kink-turn: a new RNA secondary structure motif. *EMBO J.* **20**: 4214-4221.

Kurata S, Weixlbaumer A, Ohtsuki T, Shimazaki T, Wada T, Kirino Y, Takai K, Watanabe K, Ramakrishnan V, Suzuki T. 2008. Modified uridines with C5-methylene substituents at the first position of the tRNA anticodon stabilize U•G wobble pairing during decoding. *J. Biol. Chem.* **283**: 18801-18811.

Leonarski F, D'Ascenzo L, Auffinger P. 2017. Mg^{2+} ions: do they bind to nucleobase nitrogens? *Nucleic Acids Res.* **45**: 987-1004.

Lin J, Gagnon MG, Bulkley D, Steitz TA. 2015. Conformational changes of elongation factor G on the ribosome during tRNA translocation. *Cell* **160**: 219-227.

Lundberg D, Persson I, Eriksson L, D'Angelo P, De Panfilis S. 2010. Structural study of the N,N '-dimethylpropyleneurea solvated lanthanoid(III) ions in solution and solid state with an analysis of the ionic radii of lanthanoid(III) ions. *Inorg. Chem.* **49**: 4420-4432.

Marino N, Armentano D, De Munno G. 2016. Cytosine and 1-methylcytosine Mg(II) complexes: Structural insights on the reactivity of magnesium(II) toward nucleic acid constituents. *Inorg. Chim. Acta* **452**: 229-237.

Melnikov SV, Soll D, Steitz TA, Polikanov YS. 2016. Insights into RNA binding by the anticancer drug cisplatin from the crystal structure of cisplatin-modified ribosome. *Nucleic Acids Res.* **44**: 4978-4987.

Noeske J, Huang J, Olivier NB, Giacobbe RA, Zambrowski M, Cate JH. 2014. Synergy of streptogramin antibiotics occurs independently of their effects on translation. *Antimicrob. Agents Chemother.* **58**: 5269-5279.

Noeske J, Wasserman MR, Terry DS, Altman RB, Blanchard SC, Cate JH. 2015. High-resolution structure of the *Escherichia coli* ribosome. *Nat. Struct. Mol. Biol.* **22**: 336-341.

Ogle JM, Murphy FV, Tarry MJ, Ramakrishnan V. 2002. Selection of tRNA by the ribosome requires a transition from an open to a closed form. *Cell* **111**: 721-732.

Olieric V, Weinert T, Finke AD, Anders C, Li D, Olieric N, Borca CN, Steinmetz MO, Caffrey M, Jinek M et al. 2016. Data-collection strategy for challenging native SAD phasing. *Acta Cryst.* **D72**: 421-429.

Perez-Fernandez D, Shcherbakov D, Matt T, Leong NC, Kudyba I, Duscha S, Boukari H, Patak R, Dubbaka SR, Lang K et al. 2014. 4'-O-substitutions determine selectivity of aminoglycoside antibiotics. *Nat. Commun.* **5**: 3112.
Petrov AS, Bernier CR, Hershkovits E, Xue YZ, Waterbury CC, Hsiao CL, Stepanov VG, Gaucher EA, Grover MA, Harvey SC et al. 2013. Secondary structure and domain architecture of the 23S and 5S rRNAs. *Nucleic Acids Res.* **41**: 7522-7535.
Polikanov YS, Blaha GM, Steitz TA. 2012. How hibernation factors RMF, HPF, and YfiA turn off protein synthesis. *Science* **336**: 915-918.
Polikanov YS, Melnikov SV, Soll D, Steitz TA. 2015a. Structural insights into the role of rRNA modifications in protein synthesis and ribosome assembly. *Nat. Struct. Mol. Biol.* **22**: 342-344.
Polikanov YS, Osterman IA, Szal T, Tashlitsky VN, Serebryakova MV, Kusochek P, Bulkley D, Malanicheva IA, Efimenko TA, Efremenkova OV et al. 2014a. Amicoumacin A inhibits translation by stabilizing mRNA interaction with the ribosome. *Mol. Cell* **56**: 531-540.
Polikanov YS, Starosta AL, Juette MF, Altman RB, Terry DS, Lu W, Burnett BJ, Dinos G, Reynolds KA, Blanchard SC et al. 2015b. Distinct tRNA accommodation intermediates observed on the ribosome with the antibiotics hygromycin A and A201A. *Mol. Cell* **58**: 832-844.
Polikanov YS, Steitz TA, Innis CA. 2014b. A proton wire to couple aminoacyl-tRNA accommodation and peptide-bond formation on the ribosome. *Nat. Struct. Mol. Biol.* **21**: 787-793.
Polikanov YS, Szal T, Jiang F, Gupta P, Matsuda R, Shiozuka M, Steitz TA, Vazquez-Laslop N, Mankin AS. 2014c. Negamycin interferes with decoding and translocation by simultaneous interaction with rRNA and tRNA. *Mol. Cell* **56**: 541-550.
Pulk A, Cate JH. 2013. Control of ribosomal subunit rotation by elongation factor G. *Science* **340**: 1235970.
Roy RN, Lomakin IB, Gagnon MG, Steitz TA. 2015. The mechanism of inhibition of protein synthesis by the proline-rich peptide oncocin. *Nat. Struct. Mol. Biol.* **22**: 466-469.
Schmeing TM, Huang KS, Kitchen DE, Strobel SA, Steitz TA. 2005a. Structural insights into the roles of water and the 2' hydroxyl of the P site tRNA in the peptidyl transferase reaction. *Mol. Cell.* **20**: 437-448.
Schmeing TM, Huang KS, Strobel SA, Steitz TA. 2005b. An induced-fit mechanism to promote peptide bond formation and exclude hydrolysis of peptidyl-tRNA. *Nature* **438**: 520-524.
Schmeing TM, Moore PB, Steitz TA. 2003. Structures of deacylated tRNA mimics bound to the E site of the large ribosomal subunit. *RNA* **9**: 1345-1352.
Schroeder SJ, Blaha G, Moore PB. 2007a. Negamycin binds to the wall of the nascent chain exit tunnel of the 50S ribosomal subunit. *Antimicrob. Agents Chemother.* **51**: 4462-4465.
Schroeder SJ, Blaha G, Tirado-Rives J, Steitz TA, Moore PB. 2007b. The structures of antibiotics bound to the E site region of the 50 S ribosomal subunit of Haloarcula marismortui: 13-deoxytedanolide and girodazole. *J. Mol. Biol.* **367**: 1471-1479.
Seefeldt AC, Graf M, Perebaskine N, Nguyen F, Arenz S, Mardirossian M, Scocchi M, Wilson DN, Innis CA. 2016. Structure of the mammalian antimicrobial peptide Bac7(1-16) bound within the exit tunnel of a bacterial ribosome. *Nucleic Acids Res.* **44**: 2429-2438.
Selmer M, Dunham CM, Murphy FV, Weixlbaumer A, Petry S, Kelley AC, Weir JR, Ramakrishnan V. 2006. Structure of the 70S ribosome complexed with mRNA and tRNA. *Science* **313**: 1935-1942.
Sigel RK, Skilandat M, Sigel A, Operschall BP, Sigel H. 2013. Complex formation of cadmium with sugar residues, nucleobases, phosphates, nucleotides, and nucleic acids. *Met. Ions Life Sci.* **11**: 191-274.
Simonovic M, Steitz TA. 2008. Peptidyl-CCA deacylation on the ribosome promoted by induced fit and the O3 '-hydroxyl group of A76 of the unacylated A-site tRNA. *RNA* **14**: 2372-2378.
Sugawara Y, Kamiya N, Iwasaki H, Ito T, Satow Y. 1991. Humidity-controlled reversible structure transition of disodium adenosine 5'-triphosphate between dihydrate and trihydrate in a single-crystal state. *J. Am. Chem. Soc.* **113**: 5440-5445.
Thuery P. 2009. Lanthanide complexes with cucurbit[n]urils (n = 5, 6, 7) and perrhenate ligands: new examples of encapsulation of perrhenate anions. *Inorg. Chem.* **48**: 4497-4513.
Tourigny DS, Fernandez IS, Kelley AC, Ramakrishnan V. 2013. Elongation factor G bound to the ribosome in an intermediate state of translocation. *Science* **340**: 1235490.
Tu D, Blaha G, Moore PB, Steitz TA. 2005. Structures of MLSBK antibiotics bound to mutated large ribosomal subunits provide a structural explanation for resistance. *Cell* **121**: 257-270.
Vendeix FA, Murphy FVt, Cantara WA, Leszczynska G, Gustilo EM, Sproat B, Malkiewicz A, Agris PF. 2012. Human tRNA(Lys3)(UUU) is pre-structured by natural modifications for cognate and wobble codon binding through keto-enol tautomerism. *J. Mol. Biol.* **416**: 467-485.
von Bohlen K, Makowski I, Hansen HA, Bartels H, Berkovitch-Yellin Z, Zaytzev-Bashan A, Meyer S, Paulke C, Franceschi F, Yonath A. 1991. Characterization and preliminary attempts for derivatization of crystals of large ribosomal subunits from *Haloarcula marismortui* diffracting to 3 A resolution. *J. Mol. Biol.* **222**: 11-15.
Weixlbaumer A, Murphy FVt, Dziergowska A, Malkiewicz A, Vendeix FA, Agris PF, Ramakrishnan V. 2007. Mechanism for expanding the decoding capacity of transfer RNAs by modification of uridines. *Nat. Struct. Mol. Biol.* **14**: 498-502.
Wimberly BT, Brodersen DE, Clemons WM, Jr., Morgan-Warren RJ, Carter AP, Vonrhein C, Hartsch T, Ramakrishnan V. 2000. Structure of the 30S ribosomal subunit. *Nature* **407**: 327-339.
Wimberly BT, Guymon R, McCutcheon JP, White SW, Ramakrishnan V. 1999. A detailed view of a ribosomal active site: the structure of the L11-RNA complex. *Cell* **97**: 491-502.
Zhang J, Ferre-D'Amare AR. 2014. Dramatic improvement of crystals of large RNAs by cation replacement and dehydration. *Structure* **22**: 1363-1371.
Zheng H, Shabalin IG, Handing KB, Bujnicki JM, Minor W. 2015. Magnesium-binding architectures in RNA crystal structures: validation, binding preferences, classification and motif detection. *Nucleic Acids Res.* **43**: 3789-3801.